256–266 *Nucleic Acids Research, 2018, Vol. 46, No. 1* *Published online 22 November 2017*
doi: 10.1093/nar/gkx1149

Mechanism of formation of a toroid around DNA by the mismatch sensor protein

Shivlee Nirwal[1,2], Dhananjaya S. Kulkarni[3], Amit Sharma[4], Desirazu N. Rao[3] and Deepak T. Nair[1,*]

[1]Regional Centre for Biotechnology, NCR Biotech Science Cluster, 3rd Milestone, Faridabad-Gurgaon Expressway, Faridabad, 121001, Haryana, India, [2]Manipal University, Manipal, 576104, Karnataka, India, [3]Department of Biochemistry, Indian Institute of Science, Bangalore, 560012, Karnataka, India and [4]TERI-DIAKEN Nanobiotechnolgy Centre, TERI-Gram, Gual Pahari, Gurgaon-Faridabad Road, Gurgaon, 122001, Haryana, India

Received April 03, 2017; Revised October 26, 2017; Editorial Decision October 27, 2017; Accepted November 01, 2017

ABSTRACT

The DNA mismatch repair (MMR) pathway removes errors that appear during genome replication. MutS is the primary mismatch sensor and forms an asymmetric dimer that encircles DNA to bend it to scan for mismatches. The mechanism utilized to load DNA into the central tunnel was unknown and the origin of the force required to bend DNA was unclear. We show that, in absence of DNA, MutS forms a symmetric dimer wherein a gap exists between the monomers through which DNA can enter the central tunnel. The comparison with structures of MutS–DNA complexes suggests that the mismatch scanning monomer (B_m) will move by nearly 50 Å to associate with the other monomer (A_m). Consequently, the N-terminal domains of both monomers will press onto DNA to bend it. The proposed mechanism of toroid formation evinces that the force required to bend DNA arises primarily due to the movement of B_m and hence, the MutS dimer acts like a pair of pliers to bend DNA. We also shed light on the allosteric mechanism that influences the expulsion of adenosine triphosphate from A_m on DNA binding. Overall, this study provides mechanistic insight regarding the primary event in MMR i.e. the assembly of the MutS–DNA complex.

INTRODUCTION

The mismatch repair (MMR) pathway removes errors that appear during replication (1–4). MMR pathway initiates correction of mispairs, insertions or deletions that have escaped proofreading during DNA replication. Perturbation of this pathway results in a 100- to 1000-fold enhancement in the frequency at which mutations appear in *Escherichia coli* (2). The fact that the onset of Hereditary Non Polyposis Colorectal Cancer, Oral Squamous Cell Carcinoma and gliomas in humans are strongly co-related with mutations in MMR genes, highlights the importance of this pathway (5–8). Among specific proteins of the MMR system, MutS is responsible for detecting non-Watson–Crick base pairs in newly synthesized DNA (9). Structural and biophysical studies have shown that the functional form of MutS and orthologues is an oval, disc-shaped, asymmetric dimer (10–14). Two monomers associate to form an oval disc with a central channel into which DNA is loaded to be scanned for mismatches. The structures of MutS from *Thermus aquaticus* (TqMutS) and *E. coli* (EcMutS) in complex with DNA bearing a mismatch show that bound DNA is encircled and bent, and these attributes are vital for recognition of mismatches (11–13). MutS is an asymmetric dimer in the DNA-bound state and only one of the monomer makes base-specific contacts through the minor groove of DNA (monomer B) while the corresponding residues from the other monomer are involved in non-pecific contacts with the DNA phosphate backbone (monomer A). Single molecule microscopy studies on TqMutS suggest that the MutS monomers exhibit vibrational motion in the absence of DNA, which reduces considerably on adenosine triphosphate (ATP) binding (15,16) and that MutS translocates on DNA to scan for mismatches (17,18). However, it is still not known how the MutS–DNA complex is assembled. In the functional state of MutS, DNA is encircled by MutS dimer and it is unclear how DNA is loaded into the scanning tunnel of the MutS clamp. The processivity factor involved in DNA replication (dimeric β-clamp in prokaryotes and trimeric PCNA in eukaryotes) and the Ku protein (involved in double-stranded break repair) represent other toroidal proteins that encircle DNA (19,20). In the case of the processivity factor, a five subunit clamp loader enzyme opens the clamp dimer/trimer to load DNA into the central channel (21). The Ku protein is thought to slide onto DNA at the end generated by a double-stranded break (22). There is no known enzymatic activity that aids

*To whom correspondence should be addressed. Tel: +91 129 284 8844; Fax: +91 129 284 8803; Email: deepak@rcb.res.in

loading of the MutS clamp on DNA and therefore unlike β-clamp/PCNA, this enzyme may not require any *trans* factors. To understand the mechanism of assembly of the MutS–DNA complex, we have utilized the MutS homologue from *Neisseria gonorrhoeae*- named NgoS- as a model enzyme. NgoS has been shown to participate in MMR in *Neisseria* through detection of mismatches and small insertions or deletions (23).

In the present study, we have obtained structural information regarding the NgoS dimer in complex with Adenosine Diphosphate (ADP) and in the absence and presence of DNA using Macromolecular Crystallography (MX) and small angle X-ray scattering (SAXS), respectively. The structural analysis shows that in the absence of DNA, there exists a gap between the monomers through which DNA can enter the central tunnel. On entry, the DNA probably associates non-specifically with one monomer (A_m) and this designates the other monomer as the mismatch scanning monomer (B_m), which moves by nearly 50 Å to associate with A_m. Consequently the N-terminal domains of both monomers press onto DNA to bend it. In line with this mechanism, Dynamic Light Scattering (DLS) studies show that NgoS undergoes a compaction in the presence of DNA and that ATP binding, and not hydrolysis, is critical for this transition. Structural analysis and fluorescence anisotropy studies show that DNA binding involves expulsion of ATP from the A_m monomer. Overall, the study provides insight regarding the structural transitions in MutS on DNA binding that enable formation of the dimer clamp around DNA. The study also sheds light on the allosteric mechanism that influences the dynamics of ATP binding in the presence of DNA.

MATERIALS AND METHODS

Cloning, expression and purification of WT and mutant NgoS

The gene segment corresponding to the *mutS* gene from *N. gonorrhoeae was* amplified by polymerase chain reaction using primer sequences derived from the 5′- and 3′- ends of the open reading frames obtained from the genomic DNA. The amplified product (*ngoS*) was cloned in pGEX_6P1, using the BamHI/XhoI sites to produce a fusion polypeptide with N-terminal Glutathione S-transferase (GST) tag attached to the NgoS by a linker with the *PreScission* protease site. The authenticity of the cloned gene was confirmed by DNA sequencing. Then a truncated construct NgoSΔC814 (1–814) was generated by mutating codon corresponding to 815th residue to stop codon, referred as GST-NgoS in the paper. The GST-NgoS fusion protein was over expressed in the *Escherichia coli* C41(DE3) strain. Five litres of LB medium (100 μg/ml ampicillin) were induced with 0.1 mM of Isopropyl β-D-1-thiogalactopyranoside for 18 h at 18°C at 150 rpm. Cells were harvested by centrifugation and resuspended in buffer A [25 mM Tris–Cl (pH 8.0 at 4°C), 500 mM NaCl, 5% glycerol, 2 mM dithiothreitol, 0.01% IGEPAL CA-630 and 1 mM phenylmethylsulfonyl fluoride]. Cells were lysed by sonication followed by centrifugation at 17 000 rpm to remove cell debris. The recombinant protein was purified from the supernatant primarily using GST-sepharose (GE Healthcare Inc.). The column was pre-equilibrated with buffer B [Tris–Cl (pH 8.0 at 4°C), 250 mM NaCl, 5% glycerol, 2 mM dithiothreitol (DTT) and 0.01% IGEPAL CA-630]. Lysate was loaded on to column followed by washing with buffer C [Tris–Cl (pH 8.0 at 4°C), 1M NaCl, 5% glycerol, 2 mM DTT and 0.01% IGEPAL CA-630]. Protein was eluted using 15 mM reduced glutathione in buffer B and incubated with *PreScission* protease to cleave the tag and release the native protein (NgoS). The cleaved protein was analyzed by sodium dodecyl sulphate-polyacrylamide gel electrophoresis (SDS-PAGE), concentrated and further purified by size exclusion chromatography. Superdex-200 column (GE Healthcare Inc.) was used with buffer containing 25 mM Tris–Cl (pH 8.0 at 4°C), 500 mM NaCl, 5% glycerol and 2 mM dithiothreitol. Eluted fractions were analyzed for purity by SDS-PAGE and fractions corresponding to pure protein were pooled and concentrated to 15 mg/ml, aliquoted, flash frozen and stored at −80°C.

The catalytic mutant for the ATPase activity of NgoS was generated by site directed mutagenesis of the catalytic residue E687, in the Walker B motif, to alanine. The resulting mutant protein was purified as mentioned above for wild-type (WT) NgoS.

Estimation of ATPase activity

The ATPase activity of NgoS WT and its mutant NgoS (E687A) was measured using an EnzChek Phosphate Assay Kit (Invitrogen) in 96 well clear bottom Costar® plates (Corning). NgoS WT and mutant (1 μM) was added to the reaction buffer with purine nucleoside phosphorylase enzyme and 2-amino-6-mercapto-7-methylpurine riboside substrate (as described in the kit), followed by an incubation for a period of 10 min at 22°C. The reaction was then started by adding ATP (2 mM) and absorbance was measured continuously at 360 nm at each 3-min interval. A standard curve was generated using K_2PO_4, as the source of inorganic phosphate, provided with the kit. The P_i released during the reaction was calculated using the standard curve thereby calculating the rate of reaction and initial velocity. The experiment was done in triplicate for both WT and the mutant.

Binding of WT and E687A mutant to heteroduplex DNA

Fluorescence anisotropy was measured for both NgoS WT and NgoS(E687A) using 31mer heteroduplex DNA with G:T mismatch. The 3′ end of one of the oligonucleotide in the duplex was labelled with 6-fluorescein amidite (6-FAM), procured from Keck Biotechnology Resource Laboratory (Yale University).

- **5′ GCGATGTTGCTGACGCTGGTGCCTGGCAGCT -6FAM 3′**
- **3′ CGCTACAACGACTGTGACCACGGACCGTCGA 5′**

The protein in varying concentration (0–100 nM) was incubated with 10 nM of respective DNA in a binding buffer with 25 mM Tris pH 8.0, 5% glycerol, 1 mM DTT, 150 mM NaCl at room temperature for 45 min. All the reactions were carried out in 96 well black bottom Costar® plates

(Corning), in triplicates. SpectraMax M5 micro plate reader (Molecular Devices) was used for measuring fluorescence anisotropy. Fluorescence anisotropy was monitored at the excitation wavelength of 492nm and emission wavelength of 517 nm and calculated by the Spectramax software using the following equation

$$FA = [(I//) - (GxI\perp)]/[(I//) + (2GxI\perp)]$$

wherein I// = Fluorescence intensity parallel; I⊥ = Fluorescence intensity perpendicular; G = G factor, (= 1.000 for the given calculations)

Average anisotropy was calculated from three independent measurements, for each protein concentration. Reduced anisotropy values for each protein concentration were calculated by subtracting the averaged anisotropy value for without protein reaction from the respective averaged anisotropy value. The reduced anisotropy values was then plotted (on *Y*-axis) against protein concentration (on *X*-axis). The reduced anisotropy was fitted to calculate the K_d values using the following logistic equation.

$$y = A2 + [(A1 - A2) / (1 + (x/x0)^p]$$

where, A2 is maximum reduced anisotropy, A1 is minimum reduced anisotropy, x0 is the *x*-value of the point of inflection, corresponding to the K_d and p is the Hill's slope of the curve.

Crystallization

NgoS (0.1 mM) was incubated with ADP (0.2 mM) or AMPPNP (0.2 mM) in presence of $MgCl_2$ (1 mM) for 2 min at 25°C followed by incubation for 30 min at 4°C for crystallization trials. Extensive screening and optimization was carried out and finally large single crystals were obtained in 10–14% (w/v) PEG 4000, 0.1M MES buffer (pH 6.5), 10–14% (v/v) glycerol and 0.1–0.2 M $MgCl_2$. Crystals were cryoprotected by soaking into reservoir solution with 5,10,15 and 20% ethylene glycol for 1 min followed by flash freezing in liquid nitrogen.

Structure determination

X-ray diffraction data was collected at BM14 beamline of the European Synchrotron Radiation Facility. NgoS-ADP and NgoS-AMPPNP crystals diffracted to a resolution of 2.97 Å and 3.3 Å, respectively. The collected data were processed and merged using data processing programs like HKL3000 (24). The structure was determined by the molecular replacement (MR) method using a monomer from the available $EcMutS_{DNA:ADP}$ complex structure (PDB code: 1E3M) as a search model. MR with Phaser provided a solution with two molecules in the asymmetric unit (25). Iterative rounds of crystallographic refinement using the PHENIX program and model building using Coot was carried out till convergence of the R-factors (26,27). Finally, Translation-Libration-Screw (TLS) refinement was carried out with the different domains defined as discrete rigid units. The final R_{free} and R_{work} values are 26.8 and 23.4%, respectively for the NgoS–ADP complex. The final R_{free} and R_{work} values are 25.9 and 21.2%, respectively for the NgoS–AMPPNP complex. All structural comparisons were done using the Superpose tool in Coot and the interactions between the clamp regions were mapped using CONTACT in CCP4 (27,28). All figures were prepared using PyMol (Schrödinger Corp.) and the movies were prepared in PyMol (Schrödinger Corp.) and Chimera (29).

Small angle X-ray scattering

Small angle X-ray scattering data were collected at BM29 BioSAXS beamline, ESRF, Grenoble. SAXS measurements were carried out for the $NgoS_{DNA:ADP}$ complex in buffer containing 25 mM TRIS pH 8.0, 150 mM NaCl, 5% Glycerol and 1 mM DTT, with ADP (0.15 mM) and MgCl2 (0.15 mM). The data were acquired at three protein concentrations (2, 3.5 and 5 mg/ml) for the $NgoS_{DNA:ADP}$ complex (DNA concentration being 1.2 molar excess of NgoS dimer). The samples and buffer blanks were centrifuged prior to the data collection at 20 000 *g* for 30 min at 4°C to remove any possible aggregates in the sample. Data collection was carried out at 10°C and a set of 10 measurements were made per sample. Buffer scattering was also collected prior to each sample measurement and was used to generate buffer subtracted intensity profiles. The data was processed using the Primus software (30) available in the data analysis suite ATSAS2.8.1 (31). The software helps to calculate two SAXS invariants, the Radius of gyration (R_g) and the Intensity at zero scattering angle ($I(0)$) using Guinier analysis. The low q range data limited by $q.R_g < 1.3$ was fitted using the straight line plot, ln $[I(q)]$ versus q^2, where q represents the scattering vector ($q = 4\pi \sin\theta/\lambda$) at scattering angle 2θ and wavelength λ of the X-ray. R_g was estimated from the slope ($R_g^{2/3}$) of the fit and $I(0)$ is the Intensity estimation where q is zero. R_g and $I(0)$ were also estimated using the GNOM program (32) that help to evaluate molecular size by plotting the pair distance distribution function (PDDF), $P(r)$, for the scattering data. $P(r)$ gives information about the shape of molecule in real-space, and approaches zero at its maximum dimension, D_{max}.

Results from GNOM were then used as inputs to generate 12 independent *ab initio* bead models of $NgoS_{DNA-ADP}$ complexes through DAMMIF software (33). These models were subsequently superimposed and averaged using DAMAVER (34). For the docking of $NgoS_{DNA:ADP}$ in to the SAXS-derived model, the structure was modelled in Coot (35) using PDB 1E3M, followed by energy minimization in Discovery Studio Client 3.5 software tool. SITUS2.8.1 was used to fit the energy minimized homology model of $NgoS_{DNA:ADP}$ into the SAXS envelope derived from the averaged bead model (36,37). Figures were generated using VMD (38).

Dynamic light scattering

DLS experiments were performed using a Zetasizer Nano ZS90 unit (Malvern Instruments Ltd). All measurements were carried out using a 12 μl cuvette at 298K. NgoS was diluted from the stock solution in buffer with 25 mM Tris–Cl (pH 8.0), 150 mM NaCl, 5% glycerol and 2 mM DTT to a concentration of 0.75 mg/ml. ADP or AMPPNP was added to a final concentration of 0.15 mM. To probe the

effect of DNA, NgoS was mixed with the following 30mer dsDNA heteroduplex (containing a G:T mismatch)

- **5′AGCTGCCAGGCACCAGTGTCAGCGTCCTAT 3′**
- **3′TCGACGGTTCGTGGTCACAGTCGCAGGATA 5′**

and homoduplex (without mismatch).

- **5′AGCTGCCAGGCACCAGTGTCAGCGTCCTAT 3′**
- **3′TCGACGGTCCGTGGTCACAGTCGCAGGATA 5′**

Protein and DNA was mixed in the ratio of 1:1.2 in the presence of 0.15 mM ADP and AMPPNP and incubated for 2 min at 25°C followed by incubation for 30 min at 4°C. The buffer, apo- protein or protein–DNA solutions were subjected to centrifugation at 14 000 rpm for 45 min immediately before measurements. The data were acquired, processed and analysed using Zetasizer software associated with the instrument to calculate hydrodynamic radius R_h values (using the Stokes Einstein equation).

Fluorescence anisotropy measurement to probe expulsion of ATP

The protein in varying concentration (0–500 nM) was incubated with 10 nM of N^6-(6-Amino)hexyl-ATP-6-FAM (Jena Bioscience GmbH) in a binding buffer (25 mM Tris–Cl pH 8.0, 5% glycerol, 500 mM NaCl and 2 mM DTT) to determine the concentration of protein NgoS where all the FAM-labelled ATP is saturated with NgoS, that turned out to be 100 nM of NgoS. Further measurements were carried out with 100 nM of NgoS.

All the reactions were carried out in 96 well black bottom Costar® plates (Corning), in triplicates. SpectraMax M5 micro plate reader (Molecular Devices) was used for measuring fluorescence anisotropy. Fluorescence anisotropy was monitored at the excitation wavelength of 492nm and emission wavelength of 517 nm and calculated by the Spectramax software from the following equation

$$FA = [(I//) - (GxI\perp)]/[(I//) + (2GxI\perp)]$$

wherein I// = Fluorescence intensity parallel, I⊥ = Fluorescence intensity perpendicular, G = G factor, (= 1.000 for the given calculations).

For monitoring the change in anisotropy in absence and presence of DNA, 100 nM of NgoS was mixed with 10 nM FAM labelled ATP alone or in presence of a 60mer dsDNA containing a G:T mismatch and a homoduplex dsDNA respectively (NgoS: DNA = 1:1.2), in the binding buffer and incubated for 90 min on ice.

- **5′CCCCTGACTCAGTTATCGTTCGTCAAGTCGAG CTGCCAGGCACCAGTGTCAGCGTCCTAT3′**
- **3′GGGGACTGAGTCAATAGCAAGCAGTTCAGCTC GACGGTTCGTGGTCACAGTCGCAGGATA5′**
- **5′CCCCTGACTCAGTTATCGTTCGTCAAGTCGAG CTGCCAGGCACCAGTGTCAGCGTCCTAT3′**
- **3′GGGGACTGAGTCAATAGCAAGCAGTTCAGCTC GACGGTCCGTGGTCACAGTCGCAGGATA5′**

The raw average anisotropy was calculated in absence and presence of DNA. The average anisotropy of free FAM-labelled ATP was also determined. Then the absolute FA in presence of DNA and absence of DNA was calculated by subtracting the FA for FAM-labelled ATP alone from the corresponding raw values

To obtain the percentage drop in anisotropy on DNA binding, the following equation was utilized,

$$\text{Percentage of anisotropy} = \frac{\text{FA in the presence of DNA}}{\text{FA in the absence of DNA}} \times 100$$

Table 1. Crystallographic data and refinement statistics for $NgoS_{ADP}$ complex

Data collection statistics	
Wavelength (Å)	0.97926
Space Group	$P2_122_1$
Cell Constants (Å)	89.1 101.6 235.2
Resolution (Å)	2.97 Å (3.047–2.97)
R_{merge}	6.4 (56.1)
I/σI	8.6 (2.0)
Completeness (%)	98.7 (99.2)
Redundancy	3.5 (3.6)
Refinement	
Resolution (Å)	50–2.97 Å
No. of Reflections	43285
R_{work}/R_{free}	23.4/26.8
No. of atoms	
Protein	11810
ADP	54
R. M. S. deviations	
Bond lengths (Å)	0.010
Bond angles (°)	1.449
Average B-factors	
Protein	70.1 (Am); 108.0 (Bm)
ADP	55.4 (Am); 83.6 (Bm)

[a]Values in parentheses are for the highest resolution shell.
[b]$R_{merge} = \Sigma|I–\langle I\rangle|/\Sigma I$, where, I is the integrated intensity of a given reflection.
[c]$R_{work} = \Sigma||F_{obs}| - |F_{calc}||/\Sigma\ |F_{obs}|$. R_{free} was calculated using 5% of data excluded from refinement.

RESULTS

Structural analysis of the $NgoS_{ADP}$ and $NgoS_{DNA:ADP}$ complexes

The E687A mutant showed very low ATPase activity compared to WT protein (Supplementary Figure S1A). The purified NgoS and the E687A mutant proteins were able to bind to heteroduplex DNA bearing a G:T mismatch (Supplementary Figure S1B). The structure of NgoS was determined bound to ADP and in the absence of DNA (Table 1). The structure shows that NgoS exists as a dimer and each monomer is composed of different domains (Figure 1A) namely N-Terminal Domain (NTD- residues 1–118), Central Domain (residues 119–403 and 534–559), Clamp region (residues 404–533) and C-Terminal domain (CTD- residues 560–785). There was clear electron density for the bound ADP molecule (Supplementary Figure S2) and is held in place due to stabilizing interactions formed with residues from the CTD (Figure 1B) including those belonging to the Walker A motif (residues 607–615: GPMGGKST). The previously determined structures of MutS–DNA complexes show that Clamp regions and CTDs from each monomer are in contact with each other to form the large central channel in which substrate DNA is loaded (11,13).

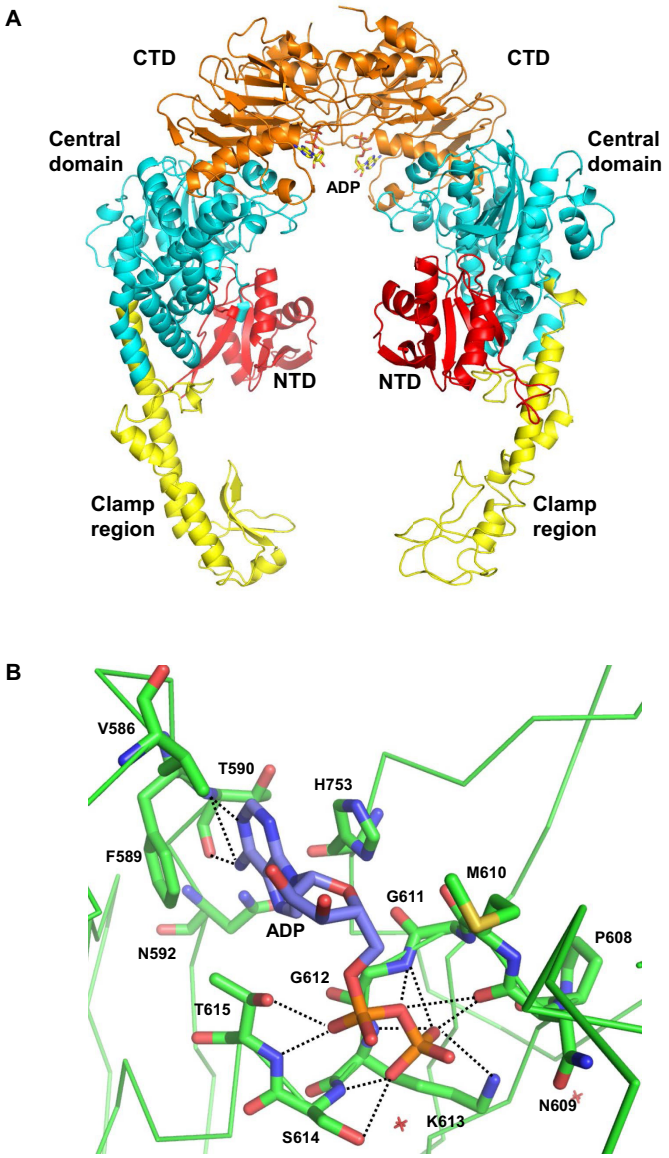

Figure 1. Structure of $NgoS_{ADP}$ complex: (**A**) Structure of $NgoS_{ADP}$ complex: The overall structure of the $NgoS_{ADP}$ complex is displayed. The N-terminal domain (NTD), Central Domain, Clamp region and the C-terminal Domain (CTD) are coloured red, cyan, yellow and brown, respectively. The ADP molecule bound to each monomer is shown in stick representation and coloured according to atom. (**B**) Interactions of ADP with NgoS: The residues of NgoS that form Van der Waals and hydrogen bonding interactions with the ADP molecule are displayed. The backbone of NgoS is displayed as ribbon and the interacting residues are shown in stick representation with C- atoms of NgoS coloured in green and that of ADP coloured in purple. The hydrogen bonds are displayed as dashed lines. The stretch 607–615 corresponds to the Walker A motif or the P-loop of NgoS.

SAXS was also used to obtain structural information regarding the $NgoS_{DNA:ADP}$ complex (Table 2). Based on the $EcMutS_{DNA:ADP}$ structure, an energy-minimized homology model of the NgoS protein in complex with DNA and ADP was used for fitting the SAXS data corresponding to the $NgoS_{DNA:ADP}$ complex. The modelled $NgoS_{DNA:ADP}$ structure fitted the SAXS envelope derived from the average bead

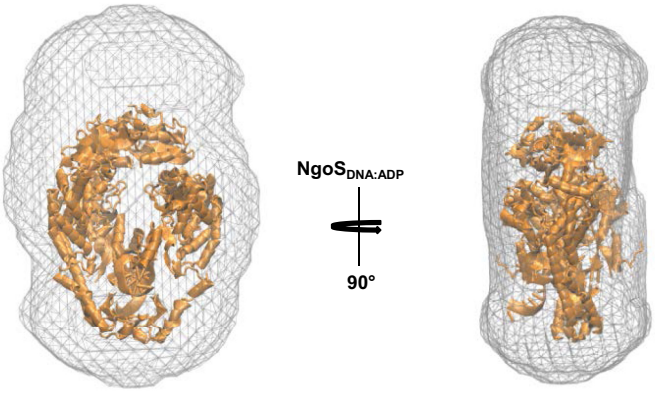

Figure 2. SAXS envelopes of the NgoS–ADP–DNA complex: Homology model of $NgoS_{DNA:ADP}$ (in orange ribbon) is superimposed with the corresponding SAXS derived *ab initio* model. The SAX envelop obtained for the complex shows that $NgoS_{DNA:ADP}$ complex adopts a shape similar to that seen for the $EcMutS_{DNA:ADP}$ and the $TqMutS_{DNA}$ complexes.

Table 2. SAX data collection and statistics

	$NgoS_{DNA:ADP}$
Data Collection parameters	
Beam line	BM29
Detector	Pilatus 1M
Wavelength (Å)	0.991
s range (nm^{-1})	0.035–4.94
Exposure time per frame (s)	0.5
No. of frames collected	10
Concentration (mg/ml)	2, 3.5, 5
Measurement Temperature (K)	283
Structural parameters	
I(0) [from P(r)]	113.30 ± 0.049
Rg (nm) [from P(r)]	6.08 ± 0.002
I(0) [from Guinier]	113.98 ± 0.96
Rg (nm) [from Guinier]	6.10 ± 0.05
Dmax (nm)	17.37

model with a correlation coefficient of ∼0.7 (Figure 2). The SAXS experiments show that the NgoS molecule adopts a conformation on binding DNA that is similar to that seen for the $EcMutS_{DNA:ADP}$ and the $TqMutS_{DNA}$ complexes.

Comparison of $NgoS_{ADP}$ structure with that of $EcMutS_{DNA:ADP}$ and $TqMutS_{DNA}$

The structure of the $NgoS_{ADP}$ complex shows drastic differences with that of MutS–DNA complex structures especially in the relative orientation of the two monomers (Figure 3 and Supplementary Figure S3). Monomer A (A_m) of $TqMutS_{DNA}$ and $EcMutS_{DNA:ADP}$ superimpose well on A_m of $NgoS_{ADP}$ complex with rmsd values of 2.3 Å (770 Cα pairs) and 2.0 Å (770 Cα pairs), respectively. This superimposition shows that the entire Monomer B (B_m) is pivoted in a different orientation in the $NgoS_{ADP}$ structure. In the DNA bound structures, the two monomers are in the same plane and form an oval disc with contacts between CTD and Clamp domains from each monomer. In the $NgoS_{ADP}$ structure, A_m and B_m are associated through CTD but are at an angle (∼45°) with respect to each other and there is no contact between residues of clamp region from each monomer (Figure 3). The comparison also shows that the

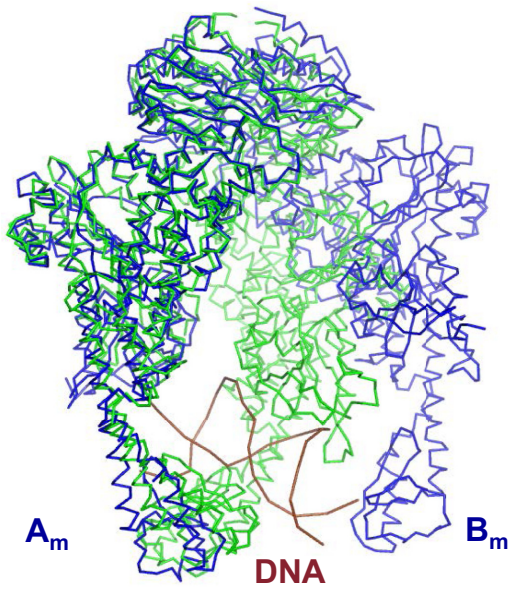

Figure 3. Comparison of $NgoS_{ADP}$ and $EcMutS_{DNA:ADP}$: a superimposition of the $NgoS_{ADP}$ and $EcMutS_{DNA:ADP}$ structures is displayed here. The $NgoS_{ADP}$ molecule is coloured blue and the $EcMutS_{DNA:ADP}$ structure is coloured green with DNA in brown. The comparison shows that there is a gap between the monomers through which DNA can enter and that monomer B_m so that the clamp regions of both monomers can interact and encircle DNA.

clamp region of A_m will have to move inwards slightly to encircle the DNA (Supplementary Figure S4).

In the $TqMutS_{DNA}$ and $EcMutS_{DNA:ADP}$ structures, it was seen that the A_m is involved in forming non-specific contacts with DNA and B_m is involved in detecting the mismatch. This partition of function leads to formation of an asymmetric dimer which is characteristic of the MutS functional complex. In line with this, A_m of $EcMutS_{DNA:ADP}$ superimposes on B_m with an rmsd of 1.4 Å. However in the case of the $NgoS_{ADP}$, A_m superimposes on B_m with an rmsd of 0.8 Å, with most of the structural differences localized to the mismatch recognizing NTD. This comparison also shows that MutS undergoes a transition from a symmetric to asymmetric dimer on DNA binding.

In $TqMutS_{DNA}$ complex, T468 of the clamp in A_m interacts with the same residue in B_m through the backbone atoms (3.1 Å). In the $NgoS_{ADP}$ structure, the corresponding residue is T488 and the distance between equivalent atoms is 48.5 Å (Figure 4). Thus, the comparison shows that in the absence of DNA, the two monomers are at angle to each other and a large gap is formed between the clamp regions from each monomer.

Structure of the $NgoS_{AMPPNP}$ complex

We were able to determine the structure of NgoS in complex with AMPPNP to a resolution of 3.3 Å (Supplementary Figure S5) (Table 3). The structure shows clear density for the AMPPNP molecule (Supplementary Figure S6) and both monomers showed the presence of one bound AMPPNP. The bound AMPPNP molecule is held in place due to stabilizing interactions formed with residues

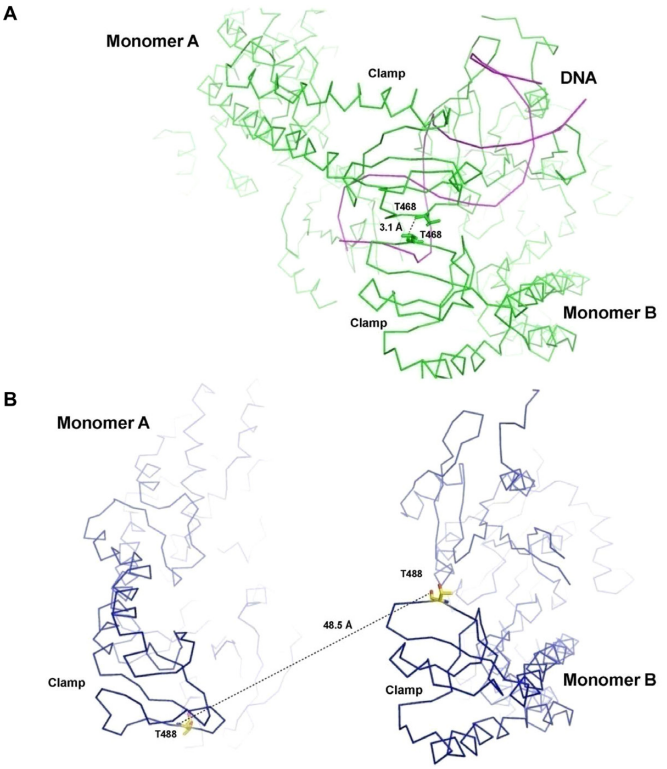

Figure 4. Comparison of the clamp regions in $NgoS_{ADP}$ and $TqMutS_{DNA}$ (**A**) The backbone atoms of the residue T468 in the clamp region of each monomer interact in $TqMutS_{DNA}$ (B) The equivalent residue T488 in monomer A of $NgoS_{ADP}$ is located 48.5 Å from the same residue in Monomer B.

from the CTD (Supplementary Figure S7). In addition to the residues that interact with ADP in the $NgoS_{ADP}$ complex, the residues D686 and E687 of the Walker B motif form interactions with the γ-phosphate of AMPPNP in the $NgoS_{AMPPNP}$ complex. The $NgoS_{AMPPNP}$ structure superimposed onto the $NgoS_{ADP}$ structure with an rmsd of 0.338 Å (1560 Cα pairs) and the structures of the two complexes are nearly identical (Supplementary Figure S8). The relative orientation of the monomers in $NgoS_{AMPPNP}$ is identical to that seen in the case of $NgoS_{ADP}$ structure and the $NgoS_{AMPPNP}$ structure also shows the presence of the gap between the clamp regions through which DNA can enter the central channel. The structure of TqMutS in its apo-state is also available and the clamp regions are disordered in this structure with no symmetry contacts between rows of molecules (Supplementary Figure S9). The comparison of TqMutS and $TqMutS_{DNA}$ structures suggests that there is only marginal difference in the orientation of the two monomers in the absence and presence of DNA. The superimposition of the two structures suggests that B_m exhibits a slight outward movement away from A_m on DNA binding and the difference in relative orientation of the two monomers that is observed in the case of $NgoS_{ADP}$ is not seen in the TqMutS structure (Supplementary Figure S10). The comparison of the TqMutS in the apo- state with the $NgoS_{ADP}$ structure suggests that on ATP binding, the two monomers attain the relative orientation seen in the case of $NgoS_{ADP}$ and the clamp regions undergo a disorder to or-

Table 3. Crystallographic data and refinement statistics for $NgoS_{AMPPNP}$ complex

Data collection statistics	
Wavelength (Å)	0.97864
Space Group	$P2_122_1$
Cell Constants (Å)	89.1 102.1 235.7
Resolution (Å)	3.3 Å (3.48–3.30)
R_{merge}	12.7 (77.5)
I/σI	8.5 (2.5)
Completeness (%)	98.1 (98.9)
Redundancy	5.3 (5.3)
Refinement	
Resolution (Å)	50–3.3 Å
No. of Reflections	32442
R_{work}/R_{free}	21.2/25.9
No. of atoms	
Protein	11820
AMPPNP	62
R.M.S. deviations	
Bond lengths (Å)	0.0011
Bond angles (°)	1.457
Average B-factors	
Protein	72.6 (Am); 108.2 (Bm)
AMPPNP	75.3 (Am); 99.5 (Bm)

[a]Values in parentheses are for the highest resolution shell.
[b]$R_{merge} = \Sigma|I-\langle I\rangle|/\Sigma I$, where I is the integrated intensity of a given reflection.
[c]$R_{work} = \Sigma||F_{obs}| - |F_{calc}||/\Sigma\,|F_{obs}|$. R_{free} was calculated using 5% of data excluded from refinement.

der transition. The overall effect of these transitions is that there is a gap formed between the two monomers and the MutS dimer now attains a state that is capable of threading DNA without the need for trans factors.

$NgoS_{ADP}$ exhibits compaction on DNA binding

Based on the crystal structures and the SAXS experiments, it appears that the NgoS transitions from an open to a closed complex on DNA entry. The presence of the gap allows DNA to enter the mismatch scanning channel. After DNA entry, the B_m will have to move by about 48 Å to be in the same flat plane as the A_m. Due to this movement the NTD from each monomer press onto the substrate DNA, and this will result in the bend observed in the DNA in MutS–DNA complexes. The bending of DNA destabilizes the helix and is vital for mismatch recognition. The proposed mechanism implies that DNA binding will involve a reduction in the hydrodynamic volume. In line with this, DLS studies showed that the addition of DNA leads to significant reduction of the hydrodynamic radius of NgoS (Figure 5). The compaction was observed in the presence of both heteroduplex and homoduplex DNA suggesting that the DNA loading process is same for mismatch scanning as well as detection.

The similarity in the structures of NgoS in complex with ADP and AMPPNP suggests that ATP hydrolysis may not be important for the DNA loading process. In agreement with this observation, the compaction was observed both in the presence of ADP and AMPPNP, implying that ATP binding, but not hydrolysis, is critical for assembly of the MutS–DNA complex (Figure 5). Mutation of the catalytic residue E687 in the Walker B motif to Ala was seen to have low ATPase activity (Supplementary Figure S1A). DLS

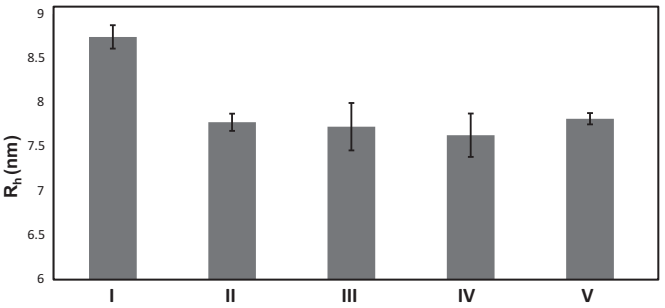

Figure 5. NgoS exhibits compaction on DNA binding. The graph displays the average R_h values obtained using DLS for (I) NgoS in the presence of ADP and absence of DNA, (II) NgoS in the presence of ADP and heteroduplex DNA bearing a G:T mismatch, (III) NgoS in the presence of AMPPNP and heteroduplex DNA bearing a G:T mismatch, (IV) NgoS in the presence of ADP and homoduplex DNA without any mismatch & (V) NgoS in the presence of AMPPNP and homoduplex DNA without any mismatch. The NgoS-ADP/AMPPNP complex undergoes significant compaction on binding DNA.

experiments showed that this mutant also exhibits compaction in the presence of DNA, further confirming that ATP hydrolysis is not critical for the DNA loading process (Supplementary Figure S11).

ATP is expelled from A_m on DNA binding

In the $NgoS_{ADP}$ structure, the ADP molecule is bound to both monomers as compared to the $EcMutS_{DNA:ADP}$ structure wherein it is only seen bound to the B_m. The ATP binding cavity in NgoS is formed by the loops 583–591, 607–615 (P-loop) and 740–755. Superimposition of the A_m of $NgoS_{ADP}$ on that of $EcMutS_{DNA:ADP}$ shows that the conformation of the loop 583–591 remains unchanged, and the loop 740–755 moves inwards towards the ATP binding cavity (Figure 6A). The P-loop exhibits maximal difference and in the conformation seen in $EcMutS_{DNA:ADP}$, the residues of this loop will clash with the phosphate moiety of the bound ADP. It is therefore possible, that the movement of the B_m towards A_m results in a conformational change in two of the loops in A_m that form the ADP binding cavity and expulsion of the bound nucleotide from the A_m.

The comparison of the $NgoS_{ADP}$ and the $EcMutS_{DNA:ADP}$ structures shows that for the mismatch binding monomer (B_m), the C-terminal helix-turn-helix (residues 760–785 in NgoS) is the only region that shows some degree of overlap in the two structures (Supplementary Figure S12). Conversely, while the rest of the monomer structure shows good overlap, the C-terminal region (CTR) made up of a hairpin and helix-turn-helix (738–779 in NgoS) of A_m does not overlap with corresponding region in $EcMutS_{DNA:ADP}$ This region of A_m appears to move downward on DNA binding and this movement forces the P-loop (residues 607–615) to enter the cavity in which the triphosphate moiety of ATP is present (Figure 6B). The residue H753 from the C-terminal hairpin and helix of NgoS forms an interaction with the backbone atom of M610 and this interaction holds the CTR and P-loop together and couples their downward movement. The residues H753 and M610 are conserved in EcMutS as

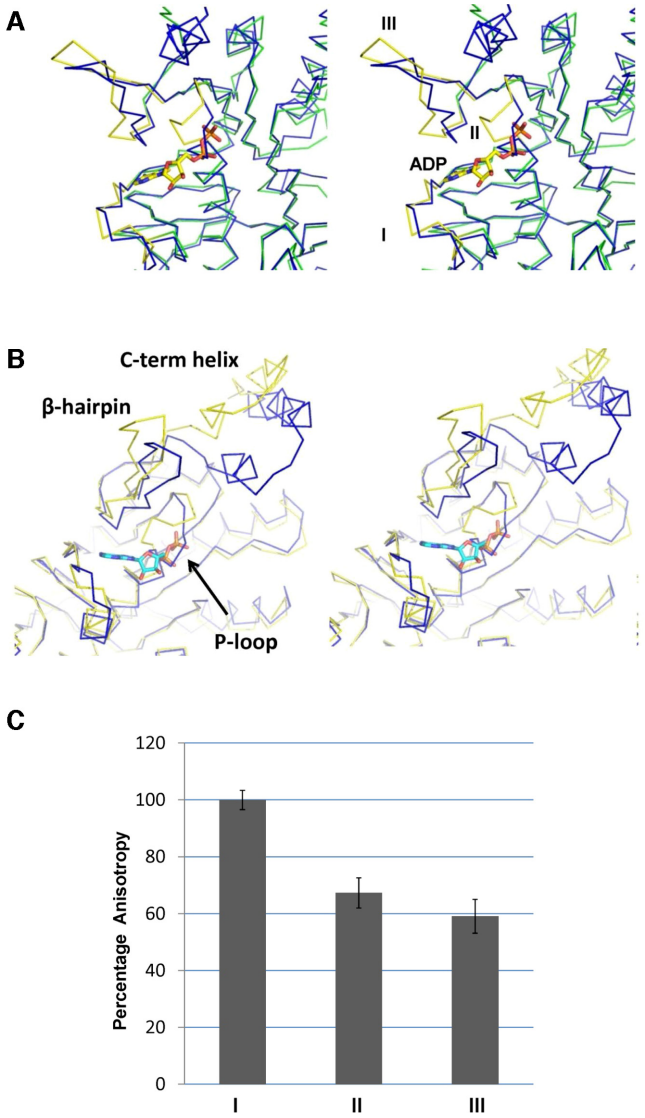

Figure 6. ATP expulsion on DNA binding: Stereo Figures showing comparison of the ADP binding site in Monomer A of $EcMutS_{DNA:ADP}$ (in blue) and $NgoS_{ADP}$ (in green). (**A**) The ATP binding loops in $NgoS_{ADP}$ are displayed in yellow with the residues 583–591, 607–615 (P-loop) and 740–755 labelled I, II and III, respectively. The P-loop appears to move inward on DNA binding and will clash with the phosphate moiety of the ADP molecule. (**B**) The repositioning of B_m (not shown here) is concomitant with a downward movement of the C-terminal helix and this ultimately results in the inward movement of the P-loop. Movie 1: the movie shows the changes in the C-terminal region (residues 740–755) and P-loop of A_m on movement of B_m. The CTR is coloured blue and the P-loop is coloured red. The final conformation attained by the P-loop in A_m will clash with the bound ATP resulting in its expulsion. (**C**) The graph displays the change in fluorescence anisotropy of 6-FAM labelled ATP (I) in the presence of NgoS and absence of DNA (II) in the presence of NgoS and presence of heteroduplex DNA bearing a G:T mismatch and (III) in the presence of NgoS and presence of homoduplex DNA without any mismatches.

H760 and M617, respectively. The comparison therefore provides insight into why the ADP is not bound to A_m in the $EcMutS_{DNA:ADP}$ structure. Overall, it appears that the CTR acts like a hinge around which B_m pivots so that the clamp regions of the two monomers can associate after DNA binding (Movie 1). Deletions in this region have been shown to adversely affect function of TqMutS (39). Regions of different lengths starting from the C-terminus were deleted and it was seen that if the TqMutS protein was truncated at or before residue 757 then the ability to dimerize was lost and consequently mismatch recognition was affected. However, TqMutS truncated till residue 760 could dimerize but transformation with this construct in a MutS deleted strain led to a mutation frequency that was higher than a MutS null strain. Our studies suggest that truncation till 760 may permit dimerization but perturb the ability of the C-terminal region to act as a hinge to enable movement of the B_m monomer and thus adversely impact mismatch recognition. Overall, the movement of B_m is coupled to the movement of C-terminal hairpin & helix in A_m which ultimately results in the expulsion of ATP from A_m.

The observed fluorescence anisotropy due to binding of 6FAM- labelled ATP to NgoS or E687A mutant dropped by about 40% on the addition of heteroduplex DNA bearing a G:T mismatch (Figure 6C and Supplementary Figure S13). This observation is in line with the prediction that binding of DNA will result in expulsion of ATP/ADP molecule bound to the A_m. A similar drop for WT and mutant protein was observed in the presence of homoduplex DNA also and this suggests that ATP expulsion is part of the DNA scanning process. The $TqMutS_{DNA}$ complex structure was initially determined in the absence of ATP/ADP and soaking these crystals with ADP showed that both monomers are bound by ADP, unlike $EcMutS_{DNA:ADP}$ (14,40). It is possible that the two monomers are occupied in $TqMutS_{DNA}$ due to high concentrations of ATP/ADP used or that there are significant differences regarding the dynamics of ATP binding during MutS–DNA assembly in the case of mesophilic and thermophilic bacteria.

DISCUSSION

Based on single molecule microscopy studies, it was suggested that the MutS molecules exhibits vibrational scissoring motion with high frequency association and dissociation of the clamp regions (15). Our studies suggest that binding of ATP may reduce the frequency of these motions considerably and give rise to a more rigid structure wherein the two monomers are held at an angle to each other and not present in the same flat plane. This configuration leads to the formation of a gap between the two monomers through which DNA can be loaded onto the central channel. The MutS molecule probably loads onto DNA such that one monomer forms non-specific contacts with DNA. The other monomer- which now represents the mismatch binding monomer then has to undergo a large movement in which the clamp region of this monomer moves by as much as 50 Å to come in contact with the clamp region of the other monomer and encircle DNA. The contacts formed between DNA and the clamp regions and the NTD will ensure that the mobility in the clamp regions is abolished to form a stable toroid around DNA. FRET-based experiments showed that the distance between NTD varies and this variation reduces on DNA binding (16). It was inferred from these studies that the NTD moves inwards and outwards in the absence of DNA and in the presence

of DNA, NTD from both monomers move towards each other. In contrast to this inference, our studies suggest that the change in distance between the NTDs is due to the movement of the entire monomer as a rigid unit towards the other monomer.

In addition to the conjecture that the NTDs flip between open and closed states, it was also believed that the clamp regions are mobile in the absence of DNA. Earlier models of DNA assembly suggested that DNA slips in through the gap created due to the movement of only these clamp regions. The clamp regions were believed to exhibit an inward movement in the presence of DNA in order to associate with each other and encircle DNA (13). However, it is difficult to envision that the movement of these mobile regions can generate the force required to bend DNA and destabilize the helix to scan for mismatches. The DNA double helix is known to be rigid even over short length scales and therefore a considerable amount of force would be required to bend DNA (41). Our studies show that the entire mismatch recognizing monomer moves towards the other monomer and this will result in the NTD pressing down on DNA to bend it. The proposed mechanism suggests that the two monomers may act like the jaws of a pair of wire bending pliers and the force generated due to movement of the entire monomer should be adequate to bend DNA and destabilize the helix to scan for mismatches.

The complexes presented here show the presence of ADP/AMPPNP in the binding site of both monomers. However, in the DNA bound complexes of EcMutS, the mismatch binding monomer shows the presence of ADP but the other monomer does not (11). The studies presented here also show that the MutS–ATP complex undergoes a transition from symmetric to asymmetric complex on binding DNA. This is in contrast to earlier beliefs that the asymmetry exists in the MutS even prior to DNA binding (42). These observations imply that choice of which monomer will recognize the mismatch and which monomer will bind DNA non-specifically is arbitrary and happens stochastically in the presence of DNA. Such a situation will ensure that initially there is no polarity in the MutS dimer vis-a-vis DNA binding. This will enable MutS to load onto DNA in either orientation of the dimer (related by 180 degree rotation around the long axis) and diffuse in either direction to scan for mismatches. These attributes will ensure that the probability of finding a mismatch is independent of the location of MutS loading and dimer orientation and therefore the chances of non-detection of a mismatch are minimal. The observed asymmetry in the MutS–DNA complex manifests itself only on binding DNA and not before to optimize the chances of finding mismatches during scanning.

Overall, the structural analysis and biophysical studies shown here along with previous observations suggest the following sequence of events (Figure 7 and Movie 2): (i) MutS binds nucleotide resulting in reduced vibrational motion of the two monomers. The nucleotide binding results in the formation of a stable structure as observed in the case of $NgoS_{ADP}$. (ii) DNA enters the scanning tunnel through the gap present between the clamp regions of the two monomers. (iii) B_m moves to be in the same plane as A_m and the clamp region associate to thread the substrate DNA through the scanning tunnel. This movement also results in the release of the nucleotide bound to the A_m. (iv) Due to the movement of B_m, the NTDs from each monomer press down on DNA at both faces of the oval disc and this result in bending and destabilization of the DNA double helix. Residues of the NTD from B_m can then form base-specific contacts to detect the mismatch. Overall, the movement of the B_m appears to be the primary event that ensures encirclement and bending of DNA and therefore the MutS acts like a pair of pliers to bend DNA.

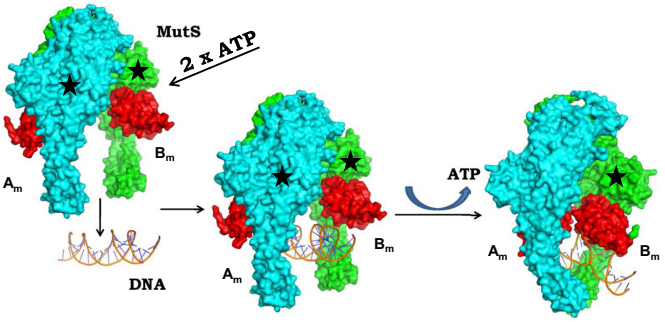

Figure 7. Mechanism of assembly of the MutS–DNA complex: The different stages in the assembly of MutS–DNA complex are displayed in. The two monomers are shown in surface representation, labelled A_m and B_m and are coloured cyan and green, respectively. The N-terminal domain of each monomer is coloured red. In addition, a movie that displays the mechanism of DNA loading onto MutS is also provided (Movie 2)**.** Movie 2: The sequence of events that occur during the assembly of the MutS–DNA complex are displayed here. The A_m and B_m monomers are shown in cyan and green colour, respectively. The P-loop of monomer Am is coloured red for the DNA is shown in ribbon representation and the bound ATP molecules are shown in stick representation.

The proposed mechanism suggests that the C-terminal region of the MutS molecule acts like a hinge to facilitate movement of the B_m towards A_m. The INSIGHT database lists all mutations in human MMR genes present and many of them co-segregate with diseases such as HNPCC. There are two MutS orthologues in eukaryotes and these molecules are heterodimers. MutSα is formed by the gene products of the *msh2* and *msh6* genes. MutSβ is formed by the gene products of msh2 and msh3 genes. The INSIGHT database lists at least 20 mutations in the msh6 gene and two mutations in the msh2 genes that will affect the region corresponding to the C-terminal helix-turn-helix of NgoS (Supplementary Table S1). This region maps to residues 1294–1335 and 798–855 in MSH6 and MSH2, respectively. It is possible that the model of MutS–DNA assembly proposed for mesophilic bacteria is conserved in eukaryotes. The mutations in the C-terminal region probably perturb the ability of MutSα to form a toroid around DNA and thus affect the efficiency of MMR in humans. In line with this hypothesis, the mutations in msh6 that lead to truncated protein that is missing the C-terminal hairpin and helix have been implicated in recurrent glioma, endometrial cancer and rectal tumour (Supplementary Table S1). Further studies on MutSα are required to validate this hypothesis and these efforts will provide deeper insight regarding mechanism of assembly of a functional MutSα–DNA complex and the effect of pathogenic mutations in the C-terminus on MMR.

DATA AVAILABILITY

The coordinates and structure factors for the $NgoS_{ADP}$ and $NgoS_{AMPPNP}$ have been deposited in the PDB with coordinates 5YK4 and 5X9W.

SUPPLEMENTARY DATA

Supplementary Data are available at NAR Online.

ACKNOWLEGEMENTS

We thank the X-ray diffraction facilities located in the Molecular Biophysics Unit of the Indian Institute of Science and at the Regional Centre for Biotechnology. D.T.N. thanks Dr Hassan Belrhali and Dr Babu Manjashetty (BM14 beamline, ESRF) for help with X-ray diffraction data collection. D.T.N. also thanks Dr Bart Van Laer (BM29 beamline, ESRF) for help with the collection of Small angle X-ray scattering data and the ESRF Access Program of RCB (supported by the Grant No. BT/INF/22/SP22660/2017 of the Department of Biotechnology, Ministry of Science and Technology).
Author contributions: Conceived and designed the experiments: D.T.N., D.N.R. Performed the experiments: S.N., D.S.K. Analyzed the data: S.N., A.S., D.T.N., D.N.R. Wrote the manuscript: S.N., D.T.N., D.N.R.

FUNDING

CSIR (Govt. of India) Senior Research Fellowship (to S.N.); DBT Research Associateship (to D.S.K.); Science & Engineering Research Board of the Department of Science & Technology, JC Bose Fellowship (to D.N.R.); Regional Centre for Biotechnology (to D.T.N.); Department of Biotechnology, Ministry of Science and Technology ['BT/PR882/BRB/10/935/2011' to D.T.N., D.N.R.]. Funding for open access charge: Regional Centre for Biotechnology, Intra-mural Grant.
Conflict of interest statement. None declared.

REFERENCES

1. Joseph,N., Duppatla,V. and Rao,D.N. (2006) Prokaryotic DNA mismatch repair. *Prog. Nucleic Acid Res. Mol. Biol.*, **81**, 1–49.
2. Watson,J.D., Baker,T.A., Bell,S.P., Gann,A., Levine,M. and Losick,R. (2013) *Molecular Biology of the Gene*. 7th edn. CSHL Press, NY.
3. Iyer,R.R., Pluciennik,A., Burdett,V. and Modrich,P.L. (2006) DNA mismatch repair: functions and mechanisms. *Chem. Rev.*, **106**, 302–323.
4. Fishel,R. (2015) Mismatch repair. *J. Biol. Chem.*, **290**, 26395–26403.
5. Xie,C., Sheng,H., Zhang,N., Li,S., Wei,X. and Zheng,X. (2016) Association of MSH6 mutation with glioma susceptibility, drug resistance and progression. *Mol. Clin. Oncol.*, **5**, 236–240.
6. Peltomaki,P. (2001) DNA mismatch repair and cancer. *Mutat. Res.*, **488**, 77–85.
7. Leach,F.S., Nicolaides,N.C., Papadopoulos,N., Liu,B., Jen,J., Parsons,R., Peltomaki,P., Sistonen,P., Aaltonen,L.A., Nystrom-Lahti,M. *et al.* (1993) Mutations of a mutS homolog in hereditary nonpolyposis colorectal cancer. *Cell*, **75**, 1215–1225.
8. Amaral-Silva,G.K., Martins,M.D., Pontes,H.A., Fregnani,E.R., Lopes,M.A., Fonseca,F.P. and Vargas,P.A. (2016) Mismatch repair system proteins in oral benign and malignant lesions. *J. Oral Pathol. Med.*, **46**, 241–245.
9. Su,S.S. and Modrich,P. (1986) Escherichia coli mutS-encoded protein binds to mismatched DNA base pairs. *Proc. Natl. Acad. Sci. U.S.A.*, **83**, 5057–5061.
10. Sixma,T.K. (2001) DNA mismatch repair: MutS structures bound to mismatches. *Curr. Opin. Struct. Biol.*, **11**, 47–52.
11. Lamers,M.H., Perrakis,A., Enzlin,J.H., Winterwerp,H.H., de Wind,N. and Sixma,T.K. (2000) The crystal structure of DNA mismatch repair protein MutS binding to a G x T mismatch. *Nature*, **407**, 711–717.
12. Natrajan,G., Lamers,M.H., Enzlin,J.H., Winterwerp,H.H., Perrakis,A. and Sixma,T.K. (2003) Structures of Escherichia coli DNA mismatch repair enzyme MutS in complex with different mismatches: a common recognition mode for diverse substrates. *Nucleic Acids Res.*, **31**, 4814–4821.
13. Obmolova,G., Ban,C., Hsieh,P. and Yang,W. (2000) Crystal structures of mismatch repair protein MutS and its complex with a substrate DNA. *Nature*, **407**, 703–710.
14. Junop,M.S., Obmolova,G., Rausch,K., Hsieh,P. and Yang,W. (2001) Composite active site of an ABC ATPase: MutS uses ATP to verify mismatch recognition and authorize DNA repair. *Mol. Cell*, **7**, 1–12.
15. Qiu,R., DeRocco,V.C., Harris,C., Sharma,A., Hingorani,M.M., Erie,D.A. and Weninger,K.R. (2012) Large conformational changes in MutS during DNA scanning, mismatch recognition and repair signalling. *EMBO J.*, **31**, 2528–2540.
16. Hingorani,M.M. (2016) Mismatch binding, ADP-ATP exchange and intramolecular signaling during mismatch repair. *DNA Repair (Amst)*, **38**, 24–31.
17. Cho,W.K., Jeong,C., Kim,D., Chang,M., Song,K.M., Hanne,J., Ban,C., Fishel,R. and Lee,J.B. (2012) ATP alters the diffusion mechanics of MutS on mismatched DNA. *Structure*, **20**, 1264–1274.
18. Jeong,C., Cho,W.K., Song,K.M., Cook,C., Yoon,T.Y., Ban,C., Fishel,R. and Lee,J.B. (2011) MutS switches between two fundamentally distinct clamps during mismatch repair. *Nat. Struct. Mol. Biol.*, **18**, 379–385.
19. Kuriyan,J. and O'Donnell,M. (1993) Sliding clamps of DNA polymerases. *J. Mol. Biol.*, **234**, 915–925.
20. Fell,V.L. and Schild-Poulter,C. (2015) The Ku heterodimer: function in DNA repair and beyond. *Mutat. Res. Rev. Mutat. Res.*, **763**, 15–29.
21. Kelch,B.A., Makino,D.L., O'Donnell,M. and Kuriyan,J. (2011) How a DNA polymerase clamp loader opens a sliding clamp. *Science*, **334**, 1675–1680.
22. Roberts,S.A. and Ramsden,D.A. (2007) Loading of the nonhomologous end joining factor, Ku, on protein-occluded DNA ends. *J. Biol. Chem.*, **282**, 10605–10613.
23. Criss,A.K., Bonney,K.M., Chang,R.A., Duffin,P.M., LeCuyer,B.E. and Seifert,H.S. (2010) Mismatch correction modulates mutation frequency and pilus phase and antigenic variation in Neisseria gonorrhoeae. *J. Bacteriol.*, **192**, 316–325.
24. Minor,W., Cymborowski,M., Otwinowski,Z. and Chruszcz,M. (2006) HKL-3000: the integration of data reduction and structure solution–from diffraction images to an initial model in minutes. *Acta Crystallogr. D Biol. Crystallogr.*, **62**, 859–866.
25. McCoy,A.J., Grosse-Kunstleve,R.W., Adams,P.D., Winn,M.D., Storoni,L.C. and Read,R.J. (2007) Phaser crystallographic software. *J. Appl. Crystallogr.*, **40**, 658–674.
26. Adams,P.D., Afonine,P.V., Bunkoczi,G., Chen,V.B., Davis,I.W., Echols,N., Headd,J.J., Hung,L.W., Kapral,G.J., Grosse-Kunstleve,R.W. *et al.* (2010) PHENIX: a comprehensive Python-based system for macromolecular structure solution. *Acta Crystallogr. D Biol. Crystallogr.*, **66**, 213–221.
27. Emsley,P.A.C.K. (2004) Coot: model building tools for molecular graphics. *Acta Crystallogr. D Biol. Crystallogr.*, **60**, 2126–2132.
28. Winn,M.D., Ballard,C.C., Cowtan,K.D., Dodson,E.J., Emsley,P., Evans,P.R., Keegan,R.M., Krissinel,E.B., Leslie,A.G., McCoy,A. *et al.* (2011) Overview of the CCP4 suite and current developments. *Acta Crystallogr. D Biol. Crystallogr.*, **67**, 235–242.
29. Pettersen,E.F., Goddard,T.D., Huang,C.C., Couch,G.S., Greenblatt,D.M., Meng,E.C. and Ferrin,T.E. (2004) UCSF Chimera–a visualization system for exploratory research and analysis. *J. Comput. Chem.*, **25**, 1605–1612.
30. Konarev,P.V., Volkov,V.V., Sokolova,A.V., Koch,M.H.J. and Svergun,D.I. (2003) PRIMUS: a Windows PC-based system for small-angle scattering data analysis. *J. Appl. Crystallogr.*, **36**, 1277–1282.

31. Franke,D., Petoukhov,M.V., Konarev,P.V., Panjkovich,A., Tuukkanen,A., Mertens,H.D.T., Kikhney,A.G., Hajizadeh,N.R., Franklin,J.M., Jeffries,C.M. *et al.* (2017) ATSAS 2.8: a comprehensive data analysis suite for small-angle scattering from macromolecular solutions. *J. Appl. Crystallogr.*, **50**, 1212–1225.
32. Svergun,D. (1992) Determination of the regularization parameter in indirect-transform methods using perceptual criteria. *J. Appl. Crystallogr.*, **25**, 495–503.
33. Franke,D. and Svergun,D.I. (2009) DAMMIF, a program for rapid ab-initio shape determination in small-angle scattering. *J. Appl. Crystallogr.*, **42**, 342–346.
34. Volkov,V.V. and Svergun,D.I. (2003) Uniqueness of ab initio shape determination in small-angle scattering. *J. Appl. Crystallogr.*, **36**, 860–864.
35. Emsley,P. and Cowtan,K. (2004) Coot: model-building tools for molecular graphics. *Acta Crystallogr. D Biol. Crystallogr.*, **60**, 2126–2132.
36. Wriggers,W. (2010) Using Situs for the integration of multi-resolution structures. *Biophys. Rev.*, **2**, 21–27.
37. Wriggers,W. (2012) Conventions and workflows for using Situs. *Acta Crystallogr. D Biol. Crystallogr.*, **68**, 344–351.
38. Humphrey,W., Dalke,A. and Schulten,K. (1996) VMD: visual molecular dynamics. *J. Mol. Graph*, **14**, 33–38.
39. Biswas,I., Obmolova,G., Takahashi,M., Herr,A., Newman,M.A., Yang,W. and Hsieh,P. (2001) Disruption of the helix-u-turn-helix motif of MutS protein: loss of subunit dimerization, mismatch binding and ATP hydrolysis. *J. Mol. Biol.*, **305**, 805–816.
40. Alani,E., Lee,J.Y., Schofield,M.J., Kijas,A.W., Hsieh,P. and Yang,W. (2003) Crystal structure and biochemical analysis of the MutS.ADP.beryllium fluoride complex suggests a conserved mechanism for ATP interactions in mismatch repair. *J. Biol. Chem.*, **278**, 16088–16094.
41. Mazur,A.K. and Maaloum,M. (2014) Atomic force microscopy study of DNA flexibility on short length scales: smooth bending versus kinking. *Nucleic Acids Res.*, **42**, 14006–14012.
42. Lamers,M.H., Winterwerp,H.H. and Sixma,T.K. (2003) The alternating ATPase domains of MutS control DNA mismatch repair. *EMBO J.*, **22**, 746–756.